

# Hydroxychloroquine is Metabolized by Cytochrome P450 2D6, 3A4, and 2C8, and Inhibits Cytochrome P450 2D6, while its Metabolites also Inhibit Cytochrome P450 3A *in vitro*<sup>§</sup>

Marie-Noëlle Paludetto,<sup>1</sup> Mika Kurkela,<sup>1</sup> Helinä Kahma, Janne T. Backman, Mikko Niemi, and Anne M. Filppula

Department of Clinical Pharmacology and Individualized Drug Therapy Research Program, Faculty of Medicine, University of Helsinki, Finland (M.-N.P., M.K., H.K., J.T.B., M.N., A.M.F.); HUS Diagnostic Center, Helsinki University Hospital, Helsinki, Finland (J.T.B., M.N.); and Pharmaceutical Sciences Laboratory, Faculty of Science and Engineering, Åbo Akademi University, Turku, Finland (A.M.F.)

Received July 1, 2022; accepted October 31, 2022

## ABSTRACT

This study aimed to explore the cytochrome P450 (CYP) metabolic and inhibitory profile of hydroxychloroquine (HCQ). Hydroxychloroquine metabolism was studied using human liver microsomes (HLMs) and recombinant CYP enzymes. The inhibitory effects of HCQ and its metabolites on nine CYPs were also determined in HLMs, using an automated substrate cocktail method. Our metabolism data indicated that CYP3A4, CYP2D6, and CYP2C8 are the key enzymes involved in HCQ metabolism. All three CYPs formed the primary metabolites desethylchloroquine (DCQ) and desethylhydroxychloroquine (DHCQ) to various degrees. Although the intrinsic clearance ( $CL_{int}$ ) value of HCQ depletion by recombinant CYP2D6 was > 10-fold higher than that by CYP3A4 (0.87 versus 0.075  $\mu\text{L}/\text{min}/\text{pmol}$ ), scaling of recombinant CYP  $CL_{int}$  to HLM level resulted in almost equal HLM  $CL_{int}$  values for CYP2D6 and CYP3A4 (11 and 14  $\mu\text{L}/\text{min}/\text{mg}$ , respectively). The scaled HLM  $CL_{int}$  of CYP2C8 was 5.7  $\mu\text{L}/\text{min}/\text{mg}$ . Data from HLM experiments with CYP-selective inhibitors also suggested relatively equal roles for CYP2D6 and CYP3A4 in HCQ metabolism, with a smaller contribution by CYP2C8. In CYP inhibition experiments, HCQ, DCQ, DHCQ, and the secondary metabolite didesethylchloroquine were

direct CYP2D6 inhibitors, with 50% inhibitory concentration ( $IC_{50}$ ) values between 18 and 135  $\mu\text{M}$ . HCQ did not inhibit other CYPs. Furthermore, all metabolites were time-dependent CYP3A inhibitors ( $IC_{50}$  shift 2.2–3.4). To conclude, HCQ is metabolized by CYP3A4, CYP2D6, and CYP2C8 *in vitro*. HCQ and its metabolites are reversible CYP2D6 inhibitors, and HCQ metabolites are time-dependent CYP3A inhibitors. These data can be used to improve physiologically-based pharmacokinetic models and update drug–drug interaction risk estimations for HCQ.

## SIGNIFICANCE STATEMENT

While CYP2D6, CYP3A4, and CYP2C8 have been shown to mediate chloroquine biotransformation, it appears that the role of CYP enzymes in hydroxychloroquine (HCQ) metabolism has not been studied. In addition, little is known about the CYP inhibitory effects of HCQ. Here, we demonstrate that CYP2D6, CYP3A4, and CYP2C8 are the key enzymes involved in HCQ metabolism. Furthermore, our findings show that HCQ and its metabolites are inhibitors of CYP2D6, which likely explains the previously observed interaction between HCQ and metoprolol.

This work was supported by the Academy of Finland (Grant decision 325667, 2019; Helsinki, Finland), Sigrid Jusélius Foundation (Grant number 8037 for J.T.B. and 1101 for M.N.), and State funding for university-level health research to HUS Helsinki University Hospital (TYH2019300 and TYH2021304 for J.T.B., TYH2019240, TYH2020323, and TYH2021324 for M.N.).

No author has an actual or perceived conflict of interest with the contents of this article.

Parts of this work were previously presented at the Pertti Neuvonen Symposium – Clinical Pharmacology and Therapeutics: from Research to Clinical Practice (November 29–30, 2021, Helsinki Finland) and at the 15<sup>th</sup> Congress of the European Association for Clinical Pharmacology and Therapeutics (June 25–28, 2022, Athens, Greece).

<sup>1</sup>Marie-Noëlle Paludetto and Mika Kurkela contributed equally to this work.

dx.doi.org/10.1124/dmd.122.001018.

§ This article has supplemental material available at [dmd.aspetjournals.org](http://dmd.aspetjournals.org).

## Introduction

The 4-aminoquinoline hydroxychloroquine (HCQ), an old antimalarial drug, is regarded as a safe and reasonably effective treatment of rheumatoid arthritis and systemic lupus erythematosus (Munster et al., 2002; Rainsford et al., 2015). Beyond its approved indications, HCQ repurposing for the prevention and treatment of various diseases, including diabetes, myocardial infarction, and various cancers, is currently assessed in several clinical trials, due to its anti-inflammatory/immunomodulating, anti-thrombotic, and anti-autophagic properties (Plantone and Koudriavtseva, 2018; Ulander et al., 2021). HCQ is preferred over chloroquine because of lower incidence of cardiac, gastrointestinal, and ocular adverse reactions. During the first stages of the Coronavirus Disease of 2019 (COVID-19) pandemic, HCQ was among the most used repurposed therapeutic agents. Although the potential benefits of systemically

**ABBREVIATIONS:** AUC, area under the concentration-time curve; BSA, bovine serum albumin; CL, clearance; CLISEF, intrinsic clearance-based intersystem extrapolation factor; COVID-19, Coronavirus Disease of 2019; CYP, cytochrome P450; DCQ, desethylchloroquine; DDCQ, didesethylchloroquine; DHCQ, desethylhydroxychloroquine;  $f_{u,mic}$ , unbound fraction in microsomes; HCQ, hydroxychloroquine; HLM, human liver microsomes; ISEF, intersystem extrapolation factor;  $K_i$ , inhibition constant;  $K_m$ , Michaelis-Menten constant;  $K_p$ , tissue-to-blood concentration coefficient or tissue-to-plasma concentration coefficient; OAT, organic anion transporter; OATP, organic anion transporting polypeptide; OCT, organic cation transporter;  $V_{max}$ , maximal velocity.

administered HCQ for the management of COVID-19 are no longer considered to outweigh its potential risks (FDA, 2020; Horby et al., 2020; Skipper et al., 2020; Pan et al., 2021), investigation of its therapeutic and prophylactic use against COVID-19 still continues (47 recruiting and not yet recruiting clinical studies as of June 15, 2022, <https://clinicaltrials.gov/>).

HCQ has been in clinical use for more than 60 years, but its clinical pharmacology is not well understood (White et al., 2020). HCQ has a complex pharmacokinetic profile, displaying a high degree of variability in its concentrations and unclear pharmacokinetic–pharmacodynamic relationships in terms of therapeutic and adverse effects (Rainsford et al., 2015). Following oral administration, approximately 70–80% of HCQ is absorbed (Tett et al., 1989). In the body, HCQ distributes extensively to aqueous cellular and intercellular compartments. As a weak base, it accumulates in acidic organelles, such as lysosomes and endosomes (Tett et al., 1993; Schrezenmeier and Dorner, 2020). Thereby, HCQ has an enormous distribution volume (700 l/kg based on plasma data) (Tett et al., 1988). HCQ also concentrates in platelets and leukocytes, leading to approximately 7-fold higher concentrations in blood than in plasma (Tett et al., 1988; Tett et al., 1989; Brocks et al., 1994). Accordingly, whole blood is frequently used as the matrix in pharmacokinetic studies (White et al., 2020). HCQ is eliminated through both metabolism and renal excretion and has a long terminal elimination half-life of 26–53 days (Tett et al., 1988; Tett et al., 1989). The full mass balance profile of HCQ is unclear, but renal elimination is estimated to account for 20–55% of the total clearance (Tett et al., 1988; Tett et al., 1989; White et al., 2020).

HCQ is biotransformed into three active metabolites in humans: the major circulating metabolite desethylhydroxychloroquine (DHCQ), as well as desethylchloroquine (DCQ), and didesethylchloroquine (DDCQ) (Fig. 1) (McChesney, 1983; Tett et al., 1985; Charlier et al., 2018; Shimizu et al., 2022). Although many articles refer to cytochrome P450 (CYP) 2C8, CYP2D6, and CYP3A4 as the key enzymes involved in HCQ metabolism, these statements are based on chloroquine data only (Kim et al., 2003; Projean et al., 2003). In addition, except for a study showing no inhibition of CYP3A4 (Li et al., 2020), little is known about the *in vitro* inhibitory effects of HCQ on CYP enzymes. In healthy

subjects, however, HCQ has increased the plasma exposure of the  $\beta$ 1 adrenergic receptor antagonist and CYP2D6 substrate metoprolol by 65% (Somers et al., 2000), suggesting that HCQ is an inhibitor of CYP2D6. These reports implying that HCQ may be both a substrate and an inhibitor of CYP2D6 raise the concern of CYP2D6 autoinhibition and thereby of time-dependent nonlinear pharmacokinetics for HCQ. Due to this concern and these gaps in the knowledge of the metabolism and drug–drug interaction potential of HCQ, this study aimed to comprehensively investigate the *in vitro* CYP-mediated metabolism of HCQ and the CYP inhibitory effects of HCQ and its three main metabolites.

## Materials and Methods

**Chemicals and Microsomes.** Hydroxychloroquine sulfate was kindly provided by Orion Corporation (Espoo, Finland). Amodiaquine dihydrochloride dihydrate, astemizole, bupropion hydrochloride, desethylchloroquine, desethylhydroxychloroquine, desethylhydroxychloroquine-d4, dextrorphan tartrate, dextrorphan-d3 tartrate, didesethylchloroquine, didesethylchloroquine-d4, hydroxybupropion, hydroxybupropion-d6, hydroxychloroquine-d4, 7-hydroxycoumarin, 7-hydroxycoumarin-d5,  $\pm$ 4-hydroxymephenytoin-d3, 1-hydroxytacrine-d3, hydroxytolbutamide, hydroxytolbutamide-d9, *N*-desethylamodiaquine hydrochloride, *N*-desethylamodiaquine-d5, *O*-desmethylastemizole, *S*-4-hydroxymephenytoin, *S*-mephenytoin, montelukast sodium, tacrine hydrochloride dihydrate, and tolbutamide were purchased from Toronto Research Chemicals (Toronto, ON, Canada). Coumarin, dextromethorphan hydrobromide monohydrate, formic acid,  $\alpha$ -hydroxymidazolam,  $\alpha$ -hydroxymidazolam-d4,  $\beta$ -NADPH tetrasodium, quinidine, and troleandomycin were bought from Sigma-Aldrich (St. Louis, MO, USA). Acetonitrile and methanol were obtained from Honeywell Riedel-de Haën (Charlotte, NC, USA), and midazolam was obtained from Hoffmann-La Roche (Basel, Switzerland). Disodium hydrogen phosphate dihydrate was purchased from Merck (Darmstadt, Germany), sodium dihydrogen phosphate monohydrate from J.T. Baker & Mallinckrodt (Deventer, The Netherlands), 1-hydroxytacrine maleate and gemfibrozil 1-*O*- $\beta$ -glucuronide from Santa Cruz Biotechnology (Dallas, TX, USA), *O*-desmethylastemizole-d4 from Medical Isotopes (Pelham, NH, USA), paroxetine hydrochloride from Synfine Research (Richmond Hill, ON, Canada), and ketoconazole from Janssen Biotech (Olen, Belgium).

Human liver microsomes (HLMs; XTreme 200 pooled, mixed-gender) used in metabolism, inhibition screening and inhibition constant ( $K_i$ ) determination experiments, and a NADPH regenerating system were purchased from Sekisui Xeno-Tech (Kansas City, KS, USA). HLMs (UltraPool 150 pooled, mixed-gender) used in  $IC_{50}$  determinations were from Corning (Woburn, MA, USA). Recombinant CYP Bactosomes (CYP1A2, CYP2A6, CYP2B6, CYP2C8, CYP2C9, CYP2C19, CYP2D6, CYP2E1, CYP2J2, CYP3A4, CYP3A5, and control Bactosomes) were from Cypex (Dundee, UK). Bovine serum albumin (BSA) was obtained from Bio-west (Nuaille, France). All solvents and commercially available reagents were of analytical grade and used without further purification.

**Incubation Conditions and Sample Handling in Metabolism Experiments.** All metabolism incubations were carried out at 37°C in sodium phosphate buffer (0.1 M, pH 7.4) in triplicate (CYP screening incubations in duplicate). HLM or recombinant CYP isoform and buffer were premixed and kept on ice until the start of the experiment. With the exception of studies including time-dependent CYP-selective inhibitors, experiments were started by premixing HCQ for 10 minutes with HLM or recombinant CYP buffer mixes on a heated shaker (37°C, 350 rpm), and followed by the addition of 1 mM NADPH to initiate the reactions. Reactions were stopped by moving a sample of the incubation mixture to acetonitrile containing internal standard (1:3). Samples were kept on ice for at least 10 minutes before centrifugation at 21,000 g for 10 minutes at 8°C and further processing (Supplemental Materials and Methods).

All stock solutions of HCQ, its metabolites, and inhibitors were prepared in methanol or acetonitrile. All incubations (including controls) contained the same concentration of organic solvent (1%). When the metabolite formation rate was measured in enzyme kinetic experiments, the incubation time was optimized within the linear range for metabolite formation, depending on the substrate turnover rate in each specific experiment (<20% turnover of substrate was required).

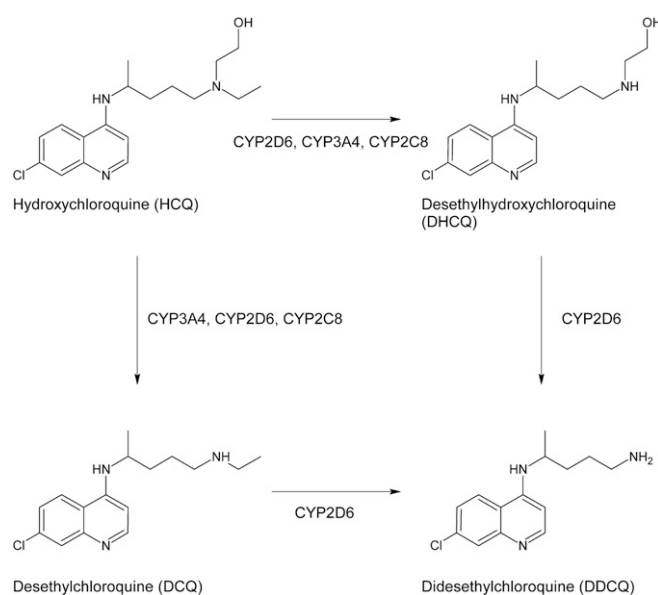


**Fig. 1.** Hydroxychloroquine main metabolic pathways, with the most important CYP enzymes indicated for each reaction, based upon the present findings. DCQ and DHCQ are primary metabolites of hydroxychloroquine, and DDCQ is formed via subsequent metabolism of either of these primary metabolites.

**Metabolism by Recombinant CYPs.** The metabolism of HCQ was first investigated in a recombinant CYP screening. HCQ (30  $\mu\text{M}$ ) was incubated with CYP enzyme (CYP1A2, CYP2A6, CYP2B6, CYP2C8, CYP2C9, CYP2C19, CYP2D6, CYP2E1, CYP2J2, CYP3A4, CYP3A5) or control Bactosomes at a protein concentration of 0.3 mg/ml with NADPH or without NADPH (negative controls) for 90 minutes. Based on the obtained data, seven CYP isoforms (CYP1A2, CYP2C8, CYP2C9, CYP2C19, CYP2D6, CYP3A4, CYP3A5) were selected for a linearity experiment. Herein, the depletion of HCQ (1 and 10  $\mu\text{M}$ ) was measured at two protein concentrations (0.1 and 0.2 mg/ml) for up to 45 minutes. Samples were collected at 0, 7.5, 15, 30, and 45 minutes. Furthermore, the depletion of HCQ at a low initial concentration of 0.3  $\mu\text{M}$  was studied in CYP2C8, CYP2D6, and CYP3A4 incubations (0.1 mg/ml). Samples were collected at the same time points as above. Finally, the enzyme kinetics of HCQ metabolite formation was tested in CYP2C8 (0.2 mg/ml), CYP2D6 (0.05 mg/ml), and CYP3A4 (0.2 mg/ml) incubations. The incubation times corresponded to 20, 10, and 20 minutes, respectively.

**Metabolism in Human Liver Microsomes.** The depletion of HCQ, DHCQ, and DCQ at initial concentrations of 0.3 and 3  $\mu\text{M}$  were also studied in HLMs (0.5 mg/ml) in the presence of NADPH. Samples were collected at 0, 15, 30, 60, 90, and 120 minutes. To study the effects of CYP inhibition on HCQ metabolism, the time-dependent inhibitors gemfibrozil 1-*O*- $\beta$ -glucuronide (75  $\mu\text{M}$ ; CYP2C8), paroxetine (15  $\mu\text{M}$ ; CYP2D6), and troleanomycin (100  $\mu\text{M}$ ; CYP3A) were first premixed with HLM (0.5 mg/ml) for 10 minutes before the addition of NADPH. After preincubation for 15 minutes, HCQ (3  $\mu\text{M}$ ) was included in the mix, and the reactions were allowed to incubate for 40 minutes. In addition, the effects of the reversible inhibitors montelukast (1  $\mu\text{M}$ ; CYP2C8), quinidine (10  $\mu\text{M}$ ; CYP2D6), and ketoconazole (1  $\mu\text{M}$ , CYP3A) were studied by premixing the inhibitor with HCQ (3  $\mu\text{M}$ ) and HLM for 10 minutes before the addition of NADPH. The reactions were allowed to incubate for 30 minutes. In an additional experiment with a low initial HCQ concentration of 0.3  $\mu\text{M}$ , the effects of the time-dependent inhibitors listed above were tested (identical incubation conditions) on HCQ depletion. Samples were collected at 0, 15, 30, 60, and 90 minutes.

**Incubation Conditions and Sample Handling in Inhibition Experiments.** The potential of HCQ, DCQ, DHCQ, and DDCQ to inhibit nine major CYP enzymes (CYP1A2, 2A6, 2B6, 2C8, 2C9, 2C19, 2D6, 2J2, and 3A) by direct inhibition, slow-binding inhibition or time-dependent inhibition was investigated in HLMs, using a previously described automated probe substrate cocktail approach (Kahma et al., 2021).

Briefly, all incubations were performed in sodium phosphate buffer (0.1 M, pH 7.4) in triplicate in 96-well plates using an automated liquid handler (Tecan Freedom EVO 150 with Freedom EVOware software, Tecan Group, Männedorf, Switzerland) and a heated shaker (550 rpm, 37°C). Probe substrates with incubation concentrations approximating to their Michaelis-Menten constant ( $K_m$ ) values were mixed into two cocktails (Supplemental Table 1) to assess several CYP activities in one experiment. The HLM protein concentrations corresponded to 0.05 mg/ml and 0.1 mg/ml for cocktail 1 and 2, respectively. BSA (0.5% (w/v), final concentration) was included in cocktail 2 incubations to enhance CYP2C19 activity. The final solvent (methanol) concentration in all incubations was  $\leq 1\%$ .

In direct inhibition incubations, the inhibitors or solvent controls, probe substrates, BSA (for cocktail 2), and HLMs were diluted in buffer, and the mixture was prewarmed on the heated shaker for 3 minutes. Incubations were initiated by the addition of NADPH (1 mM)/a NADPH regenerating system (100 mM NADP, 500 mM glucose-6-phosphate, 100 units/ml glucose-6-phosphate dehydrogenase) and terminated after 5 minutes by mixing 30  $\mu\text{l}$  of the incubation mixture with 90  $\mu\text{l}$  of ice-cold methanol containing internal standards. All samples were kept at 4°C for 30 minutes before further processing and determination of metabolite concentrations (Supplemental Materials and Methods, Supplemental Table 2).

In slow-binding inhibition incubations, the inhibitors or solvent controls were preincubated with HLMs in buffer for 30 minutes on the heated shaker. Toward the end of the preincubation, the probe substrates and BSA (for cocktail 2) were included before CYP-mediated reactions were initiated by the addition of NADPH (1 mM)/a NADPH regenerating system (100 mM NADP, 500 mM glucose-6-phosphate, 100 units/ml glucose-6-phosphate dehydrogenase). Reactions were terminated after 5 minutes, and samples were handled as described above.

In time-dependent inhibition incubations, the inhibitors or solvent controls were preincubated with HLMs and NADPH (1 mM)/a NADPH regenerating

system (100 mM NADP, 500 mM glucose-6-phosphate, 100 units/ml glucose-6-phosphate dehydrogenase) in buffer for 30 minutes on the heated shaker. Toward the end of the preincubation, BSA (for cocktail 2) was included before final incubations were initiated by adding the probe substrates. Reactions were terminated after 5 minutes, and samples were processed as described above.

**Inhibition Screening and IC<sub>50</sub> Experiments.** In an initial screening, the direct, slow-binding, and time-dependent inhibitory potential of HCQ and its metabolites were tested at two inhibitor concentrations (10 and 50  $\mu\text{M}$ ). Based on the findings, IC<sub>50</sub> experiments (direct and time-dependent inhibition) were carried out by incubating seven inhibitor concentrations (0.5–1,000  $\mu\text{M}$ ) with HLMs and the substrate cocktails. To determine the potential effect of BSA on the inhibition of the CYPs of cocktail 2, direct inhibition experiments were also carried out in the absence of BSA for HCQ and the primary metabolites.

**K<sub>i</sub> Experiments.** Based on the findings of IC<sub>50</sub> experiments, several incubations were carried out to determine the K<sub>i</sub> values for the direct inhibition of CYP2D6 and 2J2 by HCQ and its metabolites, and to characterize the type of inhibition (competitive, noncompetitive, uncompetitive, or mixed inhibition). A series of inhibitor concentrations (1/4 to 5 times the direct IC<sub>50</sub> values) were simultaneously incubated with four concentrations of dextromethorphan or astemizole ( $K_m/3$ ,  $K_m$ ,  $3 \times K_m$ , and  $9 \times K_m$ ). All incubations were performed by hand without BSA.

**Data Analysis of Metabolism Findings.** The kinetics of substrate depletion in HLM and recombinant CYP incubations was analyzed using GraphPad Prism (version 7.03; GraphPad Software, Inc., San Diego, CA, USA). Depletion rate constants ( $k_{\text{dep}}$ ) were determined using nonlinear regression, and the intrinsic clearance ( $CL_{\text{int}}$ ) of HCQ and its metabolites was expressed as  $CL_{\text{int}} = k_{\text{dep}}/[M]$ , where [M] is the HLM or recombinant CYP concentration used in the incubations. The kinetics of DCQ and DHCQ formation by CYP2C8, CYP2D6, and CYP3A4 were analyzed with the Michaelis-Menten, substrate inhibition, allosteric sigmoidal (Hill), and two enzymes models using GraphPad Prism. Selection of the best model for each reaction was based on the Akaike information criterion, R<sup>2</sup> values, and a visual examination of Michaelis-Menten and Eadie-Hofstee plots.  $CL_{\text{int}}$  values of each reaction were calculated according to  $CL_{\text{int}} = V_{\text{max}}/K_m$ , where  $V_{\text{max}}$  is the maximal velocity and  $K_m$  is the Michaelis-Menten constant.

All  $CL_{\text{int}}$  values were corrected for non-specific binding to protein by  $CL_{\text{int,u}} = CL_{\text{int}}/f_{\text{u,mic}}$ , where  $CL_{\text{int,u}}$  is the unbound intrinsic clearance and  $f_{\text{u,mic}}$  is the unbound fraction of drug at various protein concentrations.  $f_{\text{u,mic}}$  values were predicted as described in Supplemental Table 3. To estimate the relative contributions of CYP2C8, CYP2D6, and CYP3A4 to the metabolism of HCQ, Cypex LR inter-system extrapolation factors (ISEFs) and CYP expression values were obtained from the Simcyp Population-Based Simulator (V20; Simcyp Ltd, Certara, UK). The ISEFs corresponded to 0.982, 1.11, and 1.09, and the CYP expression levels to 24, 9.4, and 137 pmol/mg for CYP2C8, CYP2D6, and CYP3A4, respectively. In addition, for CYP2D6 and CYP3A4,  $CL_{\text{int}}$ -based ISEFs (CLISEFs) were calculated based on the reported marker activities for the used lots of recombinant enzymes and HLM (Proctor et al., 2004). A CLISEF value was not calculated for CYP2C8, as different marker substrates had been used for recombinant enzyme and HLM. For CYP2D6 and CYP3A4, the CLISEFs corresponded to 0.57 and 0.42, respectively. The recombinant CYP  $CL_{\text{int,u}}$  values were then multiplied with the respective ISEF or CLISEF and CYP expression value to obtain HLM  $CL_{\text{int,u}}$  values. Measured and scaled HLM  $CL_{\text{int,u}}$  values were further scaled to  $CL_{\text{int,in vivo}}$  using 39.79 mg microsomal protein/g liver, and liver volume and density values of 1.65 l and 1,080 g/l liver (Simcyp Population-Based Simulator V20). In the final step, hepatic blood clearance ( $CL_H$ ) values were calculated using the well-stirred model (Yang et al., 2007),

$$CL_H = Q_H \times \frac{f_{u,B} \times CL_{\text{int,in vivo}}}{Q_H + f_{u,B} \times CL_{\text{int,in vivo}}}$$

where  $Q_H$  is the hepatic blood flow (1.610 l/min) (Pelkonen and Turpeinen, 2007) and  $f_{u,B}$  is the unbound fraction of HCQ in blood.  $f_{u,B}$  was calculated according to  $f_{u,B} = f_{u,p} \times 1/BP$ , where  $f_{u,p}$  and BP are the unbound fraction in plasma (0.48) and blood-to-plasma concentration ratio (7.2) of HCQ, respectively (Tett et al., 1988; McLachlan et al., 1993). The calculated  $f_{u,B}$  equaled to 0.067.

**Data Analysis of Inhibition Findings.** IC<sub>50</sub> and K<sub>i</sub> values were determined by nonlinear regression using GraphPad Prism (version 8.4.3). Inhibitor concentration-response data were fitted to the following four-parameter log-logistic equation (variable slope sigmoidal model):

$$Y = \text{Bottom plateau} + \frac{\text{Top plateau} - \text{Bottom plateau}}{1 + \left(\frac{X}{IC_{50}}\right)^n}$$

where  $Y$  is the percentage of remaining CYP activity compared to the solvent controls,  $X$  is the inhibitor concentration, and  $n$  is the Hill slope. The bottom plateau was set to zero when no bottom plateau could be reliably inferred; otherwise, parameters were not constrained. In cases where a stronger CYP inhibition was observed following preincubation of the inhibitor,  $IC_{50}$  shift ( $IC_{50}$  value obtained without preincubation/ $IC_{50}$  value obtained with preincubation) values were determined. An  $IC_{50}$  shift value  $\geq 1.5$  was used to denote time-dependent inhibition.

Rate versus probe substrate concentration data were fitted to the following equations for competitive inhibition (eq. 1), noncompetitive inhibition (eq. 2), uncompetitive inhibition (eq. 3), or mixed-type inhibition (eq. 4) (Copeland, 2000):

$$v = (V_{\max} \times S) / (K_m \times (1 + [I]/K_i) + S) \quad (1)$$

$$v = (V_{\max} \times S) / (K_m + S) \times (1 + [I]/K_i) \quad (2)$$

$$v = (V_{\max} \times S) / (K_m + S \times (1 + [I]/\alpha K_i)) \quad (3)$$

$$v = (V_{\max} \times S) / (K_m \times (1 + [I]/K_i) + S \times (1 + [I]/\alpha K_i)) \quad (4)$$

where  $v$  is the velocity of the reaction,  $V_{\max}$  is the maximum velocity,  $S$  is the substrate concentration,  $K_m$  is the Michaelis constant (substrate concentration at  $V_{\max}/2$ ),  $[I]$  is the inhibitor concentration,  $K_i$  is the inhibition constant describing the affinity of the inhibitor for the enzyme, and  $\alpha K_i$  describes the affinity of the inhibitor for the enzyme-substrate complex. The type of inhibition was determined based on the Akaike information criterion and further confirmed by visual examination of Michaelis-Menten and Eadie-Hofstee plots. The latter were created by plotting the transformed data and the following lines:

$$\begin{aligned} \text{-- for direct inhibition : } y - \text{intercept} &= V_{\max}; \text{ slope} = -\alpha \\ &\times K_m, \alpha = 1 + [I]/K_i \end{aligned}$$

$$\begin{aligned} \text{-- for mixed inhibition : } y - \text{intercept} &= V_{\max} / (1 + [I]/\alpha K_i); \\ \text{slope} &= -K_m \times (1 + [I]/K_i) / (1 + [I]/\alpha K_i) \end{aligned}$$

**Prediction of Clinical Drug-Drug Interactions Due to CYP2D6 Inhibition.** The combined effects of HCQ and its metabolites on the plasma exposure of the CYP2D6 substrate metoprolol were predicted using a static mechanistic model equation (Templeton et al., 2016),

$$tAUCR = \frac{AUC_{\text{with HCQ}}}{AUC_{\text{without HCQ}}} = \left( \frac{1}{1 + \frac{[I]_{\text{HCQ}}}{K_{i,\text{HCQ}}} + \frac{[I]_{\text{DCQ}}}{K_{i,\text{DCQ}}} + \frac{[I]_{\text{DHCQ}}}{K_{i,\text{DHCQ}}} + \frac{[I]_{\text{DDCQ}}}{K_{i,\text{DDCQ}}}} \times f_m + (1 - f_m) \right)$$

where AUCR is the fold change in metoprolol area under the concentration-time curve (AUC) in the presence ( $AUC_{\text{with HCQ}}$ ) and absence ( $AUC_{\text{without HCQ}}$ ) of the perpetrators, DCQ is desethylchloroquine, DDCQ is didesethylchloroquine, DHCQ is desethylhydroxychloroquine, HCQ is hydroxychloroquine,  $[I]$  is the inhibitor concentration, and  $f_m$  is the fraction of the metoprolol dose cleared by CYP2D6. A  $f_m$  value of 0.8 was used, estimated based on clinical pharmacogenetic and interaction data available in the UW Drug Interaction Database (DIDB, Copyright University of Washington, accessed on February 11, 2021). Experimental reversible inhibition constants ( $K_i$ ) were used and adjusted for non-specific binding to HLM at 0.1 mg/ml (Supplemental Table 3). Because HCQ and its three metabolites accumulate largely in blood and tissues, six sets of interaction predictions were carried out, based on their blood (1), corresponding plasma (2), and estimated liver (3–6) concentrations. In (1), the total blood concentrations of the metabolites were estimated from HCQ concentrations and HCQ/metabolite ratios in blood (Supplemental Table 4). In (2), the corresponding total plasma concentrations of HCQ and its metabolites were calculated from their blood concentrations and blood-to-plasma values (Supplemental Table 4). In (3), their total liver concentrations were estimated from the blood concentrations and mouse tissue-to-blood concentration ( $K_p$ ) values (Chhonker et al., 2018) (Supplemental Table 4). In (4), their total liver concentrations were estimated from plasma concentrations and tissue-to-plasma partition coefficients predicted in Simcyp Population-Based Simulator V20 as described in Supplemental Table 4. In (5–6), their unbound liver concentrations were

estimated by multiplying the total liver concentrations by the unbound fraction values in plasma (thus assuming an unbound fraction in the hepatocytes that equals that observed in plasma for each compound; Supplemental Table 4).

## Results

**Metabolism in Recombinant CYP incubations.** In screening experiments, considerable HCQ depletion was observed in CYP2D6 and CYP2C8 incubations (Supplemental Fig. 1). The highest concentrations of the primary metabolites DCQ and DHCQ were formed in CYP2D6, CYP2C8, and CYP3A4 incubations (Supplemental Fig. 1). CYP3A5, CYP2C19, CYP2C9, and CYP1A2 also formed small amounts of these metabolites. The secondary metabolite DDCQ was formed abundantly in CYP2D6 incubations, while only very small amounts were produced by CYP2C8 and CYP3A4.

In follow-up experiments, when the metabolism of HCQ was studied, CYP2D6 and CYP2C8 formed the highest concentrations of HCQ primary metabolites (data of the 1  $\mu\text{M}$  HCQ/0.1 mg/ml protein experiment is shown in Fig. 2, A–D). CYP3A4 also formed smaller amounts of the metabolites. DDCQ was only formed by CYP2D6. At a low HCQ concentration of 0.3  $\mu\text{M}$ , the  $CL_{\text{int}}$  of the CYP2D6-mediated depletion of HCQ was 4.3-fold and 12-fold higher than the depletion mediated by CYP2C8 and CYP3A4, respectively (Table 1, Supplemental Fig. 2A).

DHCQ and DCQ formation by CYP2C8, CYP2D6, and CYP3A4 followed Michaelis-Menten kinetics, with evidence of substrate inhibition type kinetics in some cases (Fig. 3, A–F). CYP2D6 displayed the lowest  $K_m$  values of 20 and 7.5  $\mu\text{M}$  for DCQ and DHCQ formation, respectively.

Although the depletion rate of HCQ in recombinant CYP2D6 incubations was more than 10-fold higher than the one in CYP3A4 incubations, scaling of the recombinant data to HLM level resulted in almost equal  $CL_{\text{int}}$  values for CYP2D6 and CYP3A4, due to the much greater abundance of CYP3A4 compared with CYP2D6 (Table 1). The ISEF-based scaled HLM  $CL_{\text{int}}$  value of CYP2C8 was approximately half of those of CYP2D6 and CYP3A4.

**Metabolism in Human Liver Microsomes.** An initial HLM experiment including negative controls (no NADPH) ruled out any HCQ metabolism that would take place without external cofactors (data not shown). In HLM incubations with HCQ (3  $\mu\text{M}$ ), both its primary metabolites were formed (Fig. 4A). In HLM incubations with DCQ and DHCQ (3  $\mu\text{M}$ ) as the substrate, only DDCQ was formed (Fig. 4, B–C). In experiments with both a reversible and a time-dependent inhibitor for each enzyme, CYP2D6, CYP3A, and CYP2C8 inhibitors inhibited the formation of DHCQ from HCQ by 34–49%, 46–47%, and 27–32%, respectively (Fig. 4D). For DCQ formation, the experiments with CYP-selective reversible and time-dependent inhibitors suggested a slightly higher importance for CYP3A, with 24–44% inhibition by the CYP2D6 inhibitors, 52–57% inhibition by the CYP3A inhibitors, and 23–29% inhibition by the CYP2C8 inhibitors (Fig. 4E). In these experiments, HCQ depletion was too slow to reliably measure partial inhibition of the depletion rate by time-dependent CYP2D6, CYP3A, and CYP2C8 inhibitors (data not shown).

The depletion of HCQ, DCQ, and DHCQ at a low initial concentration of 0.3  $\mu\text{M}$  resulted in  $CL_{\text{int}}$  values of 5.6–12  $\mu\text{l}/\text{min}/\text{mg}$  (Supplemental Fig. 2B; Table 1). For HCQ, scaling of the  $CL_{\text{int}}$  resulted in a scaled hepatic clearance value of 4.1 l/h, which approximates to 71% of the published blood clearance of HCQ (Table 1).

**Inhibition Screening Using CYP Probe Substrate Cocktail Assays.** In preliminary screening experiments, HCQ was shown to cause direct inhibition of CYP2D6 (Supplemental Fig. 3); DCQ and DHCQ were direct inhibitors of CYP2D6, and of CYP2J2 to a lesser extent, as well as time-dependent inhibitors of CYP3A (Supplemental Fig. 4–5);

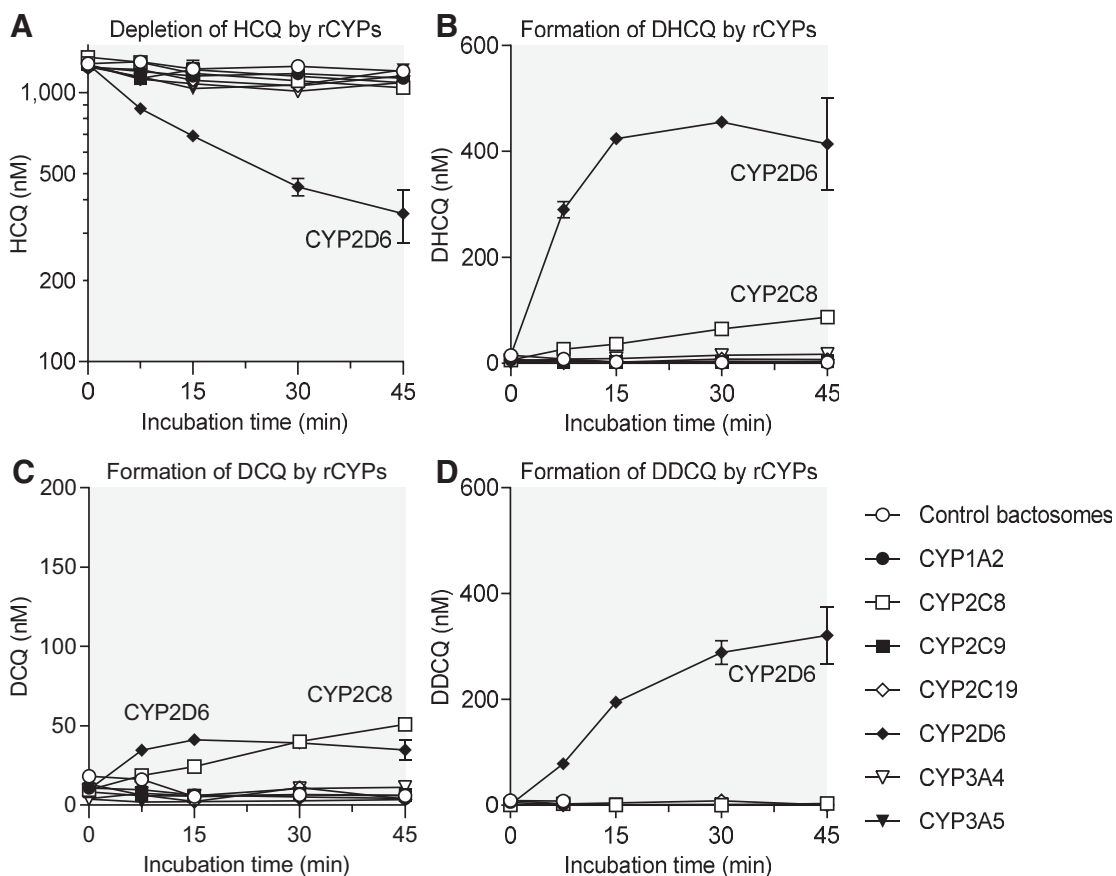


**Fig. 2.** Depletion of HCQ (1  $\mu\text{M}$ ; A) and resulting metabolite formation (B–D) in recombinant CYP incubations (0.1 mg/ml, 45 minutes). An equal protein concentration was used in parallel experiments (resulting in variable CYP contents) to keep the possible nonspecific binding of HCQ equal across incubations. The data represent mean and standard deviation values of triplicate incubations of one experiment.

while DDCQ appeared to have a broader inhibitory effect on CYP enzymes, with marked direct inhibition of CYP2D6 and CYP2J2, and time-dependent inhibition of CYP3A (Supplemental Fig. 6). There was no evidence for slow-binding inhibition of any CYP enzyme by HCQ and its metabolites (Supplemental Fig. 3–6).

**IC<sub>50</sub> Experiments Using CYP Probe Substrate Cocktail Assays.** Based on the screening data, HCQ and its metabolites were further tested for direct and time-dependent inhibition of selected CYPs. All test compounds were direct inhibitors of CYP2D6, and all three metabolites were direct inhibitors of CYP2J2, with no evidence of time-dependent inhibition (Table 2; Fig. 5, A–H). HCQ and its metabolites were moderate CYP2D6 inhibitors (IC<sub>50</sub> values ranging from 18 to 135  $\mu\text{M}$ ; Table 2), while the observed inhibition of CYP2J2 by the metabolites was in general weaker (IC<sub>50</sub> values between 63 and 504  $\mu\text{M}$ ; Table 2). Of the four compounds tested, DCQ was the most potent (direct) inhibitor of CYP2D6 (IC<sub>50</sub> = 18  $\mu\text{M}$ ), while DDCQ was the most potent (direct) inhibitor of CYP2J2 (IC<sub>50</sub> = 63  $\mu\text{M}$ ). BSA had little ( $\leq 1.3$ -fold difference) or no effect on the direct IC<sub>50</sub> values of CYP2D6 and CYP2J2 (Supplemental Table 5).

Compared with no preincubation, CYP3A inhibition increased after preincubation for 30 minutes with NADPH for all three metabolites, indicating that they are time-dependent CYP3A inhibitors (Table 2; Fig. 5, I–K; Supplemental Table 5). Preincubation of DCQ with NADPH resulted in a 3.2-fold decrease in its IC<sub>50</sub> value for CYP3A inhibition from 149  $\mu\text{M}$  to 46  $\mu\text{M}$ . Preincubation of DHCQ with NADPH had a slightly weaker effect on CYP3A inhibition, with a 2.2-fold IC<sub>50</sub> shift (from

260  $\mu\text{M}$  to 117  $\mu\text{M}$ ). DDCQ inhibited CYP3A with the lowest IC<sub>50</sub> values, with a 3.4-fold shift in IC<sub>50</sub> from 40  $\mu\text{M}$  to 12  $\mu\text{M}$  after preincubation with NADPH.

**K<sub>i</sub> Determination Experiments for CYP2D6 and CYP2J2 Direct Inhibition.** Statistical and visual examination of Michaelis-Menten and Eadie-Hofstee plots suggested that HCQ, DCQ, DHCQ, and DDCQ competitively inhibited CYP2D6 in pooled HLMs with K<sub>i</sub> values of 32.5, 10.4, 48.1, and 24.1  $\mu\text{M}$ , respectively (Fig. 6). DCQ, DHCQ, and DDCQ were mixed-type inhibitors of CYP2J2 with K<sub>i</sub> values of 382, 508, and 41.8  $\mu\text{M}$ , respectively (Fig. 7). All K<sub>i</sub> values were in good agreement with the IC<sub>50</sub> values determined during the IC<sub>50</sub> shift experiments.

**Prediction of Clinical Drug–Drug Interactions Due to Direct CYP2D6 Inhibition.** The predicted fold increase in metoprolol AUC (AUCR) following direct inhibition of CYP2D6 by HCQ and its three metabolites is shown in Fig. 8. AUCR were calculated based on HCQ, DCQ, DHCQ, and DDCQ total blood (1), total plasma (2), and total and unbound liver (3–6) concentrations. In a clinical study, administration of HCQ with metoprolol caused a 1.65-fold increase in metoprolol AUC in six patients, whose total HCQ blood concentrations ranged from 1.5 to 2.3  $\mu\text{M}$ .

Based on these blood (1) or corresponding plasma (2) concentrations (0.21–0.32  $\mu\text{M}$ ) combined with the corresponding (predicted) metabolite concentrations in blood or plasma, the predicted metoprolol AUCR was  $\leq 1.1$  (Fig. 8, A–B). However, when the corresponding (estimated) total liver concentrations (3–4) were used, the predicted metoprolol

TABLE 1  
Measured intrinsic and scaled hepatic clearance values of HCQ depletion (0.3  $\mu$ M) in HLM and recombinant CYP2C8, CYP2D6, and CYP3A4 incubations. Values shown are mean  $\pm$  standard deviation of triplicates.

Enzyme source	Scaling of HLM data			ISEF		CLISEF	
	$CL_{int}$ ( $\mu$ l/min/mg or $\mu$ l/min/pmol) <sup>a</sup>	$CL_{int}^b$ ( $\mu$ l/min/mg or $\mu$ l/min/pmol) <sup>a</sup>	HLM $CL_{int,u}$ ( $\mu$ l/min/mg)	$CL_{Ht}$ (l/h) <sup>c</sup>	$CL_{Ht}$ (l/h) <sup>c</sup>	HLM $CL_{int,u}^e$ ( $\mu$ l/min/mg)	$CL_{Ht}$ (l/h) <sup>c</sup>
HLM	$7.47 \pm 1.54$	$15.1 \pm 3.10$	$15.1 \pm 3.10$	$4.08 \pm 0.81$	71	$5.67 \pm 0.97$	n/a
CYP2C8	$0.200 \pm 0.034$	$0.241 \pm 0.042$		$1.58 \pm 0.27$	28	$5.57 \pm 0.59$	n/a
CYP2D6	$0.870 \pm 0.092$	$1.05 \pm 0.11$		$3.00 \pm 0.31$	52	$5.23 \pm 0.99$	$1.55 \pm 0.16$
CYP3A4	$0.0752 \pm 0.0142$	$0.0905 \pm 0.0170$		$3.69 \pm 0.67$	64		$1.46 \pm 0.27$

$CL_{Ht}$ , hepatic clearance;  $CL_{int}$ , intravenous clearance.

<sup>a</sup>  $\mu$ l/min/mg for HLM,  $\mu$ l/min/pmol for recombinant CYP.

<sup>b</sup> These values have been corrected for non-specific binding to protein according to  $CL_{int,u} = CL_{int}/f_{unbound}$  ( $f_{unbound}$  was estimated at a protein concentration of 0.5 mg/ml in HLM incubations, and 0.1 mg/ml in recombinant CYP incubations) (Supplemental Table 3).

<sup>c</sup> These values were calculated from HLM  $CL_{int,u}$  using equations from Yang et al. (2007).

<sup>d</sup> Intravenous blood clearance value obtained from Tett et al. (1988).

<sup>e</sup> For recombinant enzyme data, these values were obtained by multiplying recombinant CYP  $CL_{int,u}$  values with their respective ISEF and CYP expression values, or with their respective CLISEF and CYP expression values (CYP2D6 and CYP3A4).

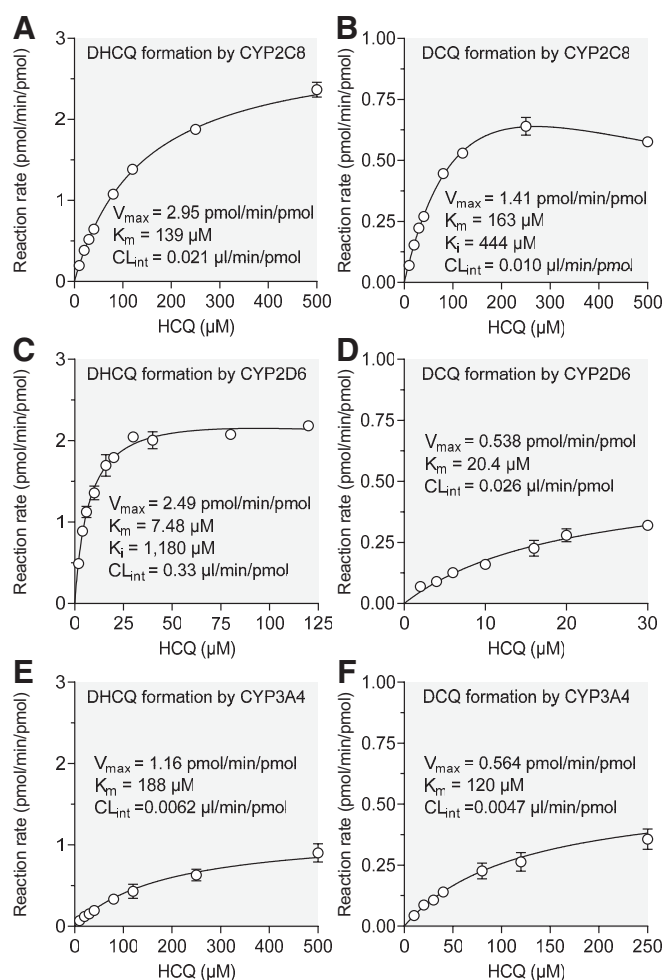


Fig. 3. Enzyme kinetics of DCQ and DHCQ formation in recombinant CYP2C8, CYP2D6, and CYP3A4 incubations (A–F). Data represent mean and standard deviation values of triplicate incubations of one experiment.

AUCR values exceeded 2.9 at the clinically relevant HCQ concentrations (Fig. 8, C–D). On the other hand, with the corresponding unbound liver concentrations (5–6), the predicted AUCR values were slightly lower (2.2–2.8) (Fig. 8, E–F). In all predictions, the contribution of metabolites was significant.

## Discussion

Until now, there has been little direct evidence of the interactions of HCQ with CYP enzymes. In the present study, we thoroughly screened the CYP-mediated metabolism of HCQ, and tested the reversible and time-dependent inhibitory effects of HCQ and its three main metabolites on nine drug-metabolizing CYPs. Our collective findings from HLMs and recombinant enzymes suggest that HCQ is mainly metabolized by CYP3A4, CYP2D6, and CYP2C8. In addition, HCQ and its metabolites are reversible, competitive inhibitors of CYP2D6, and all three HCQ metabolites are mixed-type inhibitors of CYP2J2 and time-dependent inhibitors of CYP3A.

In the literature, CYP2D6, CYP3A4, and CYP2C8 are often claimed to be the enzymes responsible for HCQ metabolism. However, these studies generally refer to chloroquine data reported by Kim et al. (2003) and Projean et al. (2003). The present findings show for the first time that these same enzymes are, indeed, also responsible for HCQ metabolism. Although the HCQ depletion rate in recombinant CYP2D6

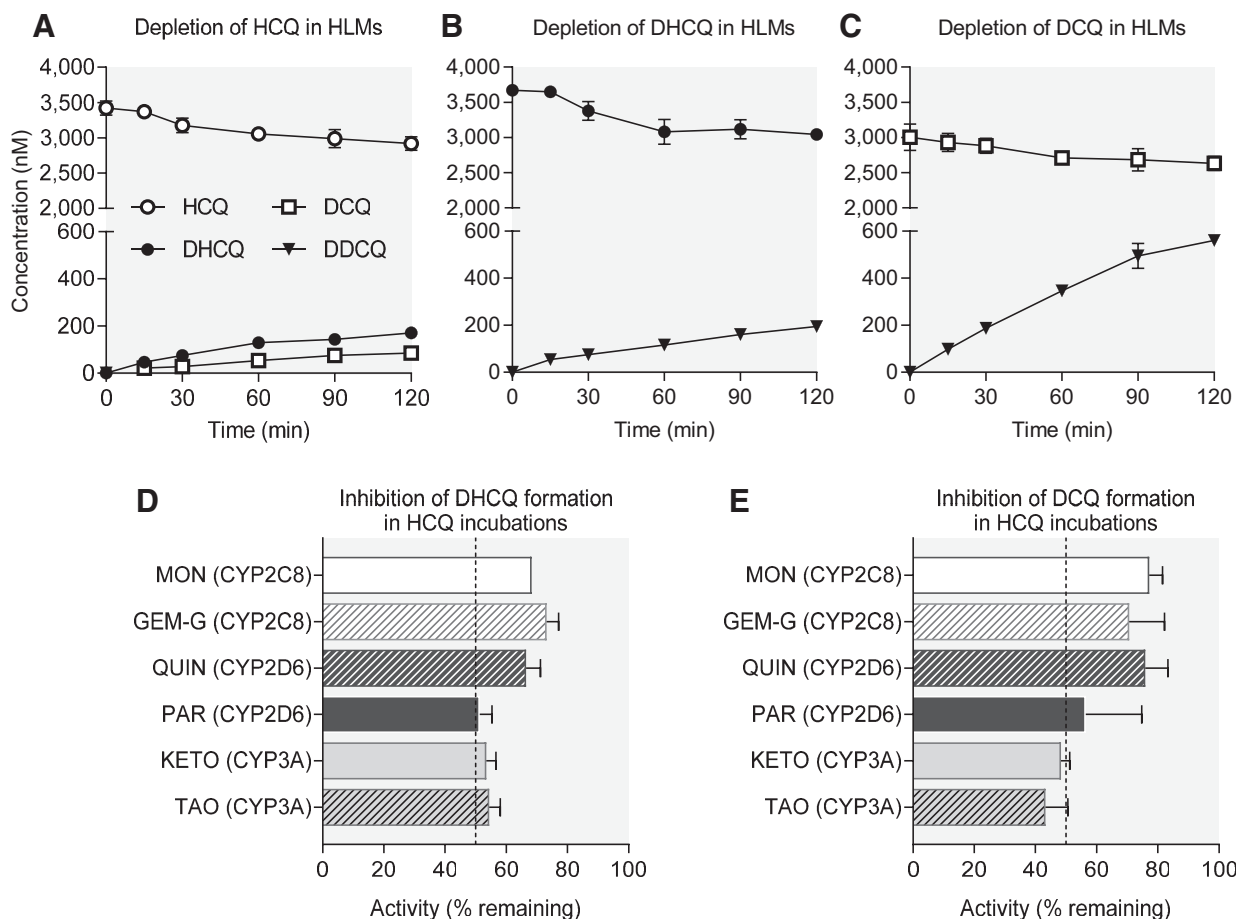


**Fig. 4.** Depletion and CYP-selective inhibition experiments in HLMs. The depletion of HCQ 3  $\mu$ M (A), DHCQ 3  $\mu$ M (B), and DCQ 3  $\mu$ M (C), and resulting metabolite formation in HLM incubations (0.5 mg/ml, 120 minutes) are shown in the top panel. In the bottom panel, the effects of CYP-selective reversible and time-dependent inhibitors on DHCQ (D) and DCQ (E) formation from HCQ (3  $\mu$ M) are illustrated. The data represent mean and standard deviation values of triplicate incubations of one experiment. GEM-G, gemfibrozil 1-O- $\beta$ -glucuronide; KETO, ketoconazole; MON, montelukast; QUIN, quinidine; PAR, paroxetine; TAO, troleandomycin.

incubations was more than 10-fold higher than that in CYP3A4 incubations, scaling of the data to the HLM level resulted in almost equal  $CL_{int}$  values for CYP2D6 and CYP3A4 (Table 1). Depending on the

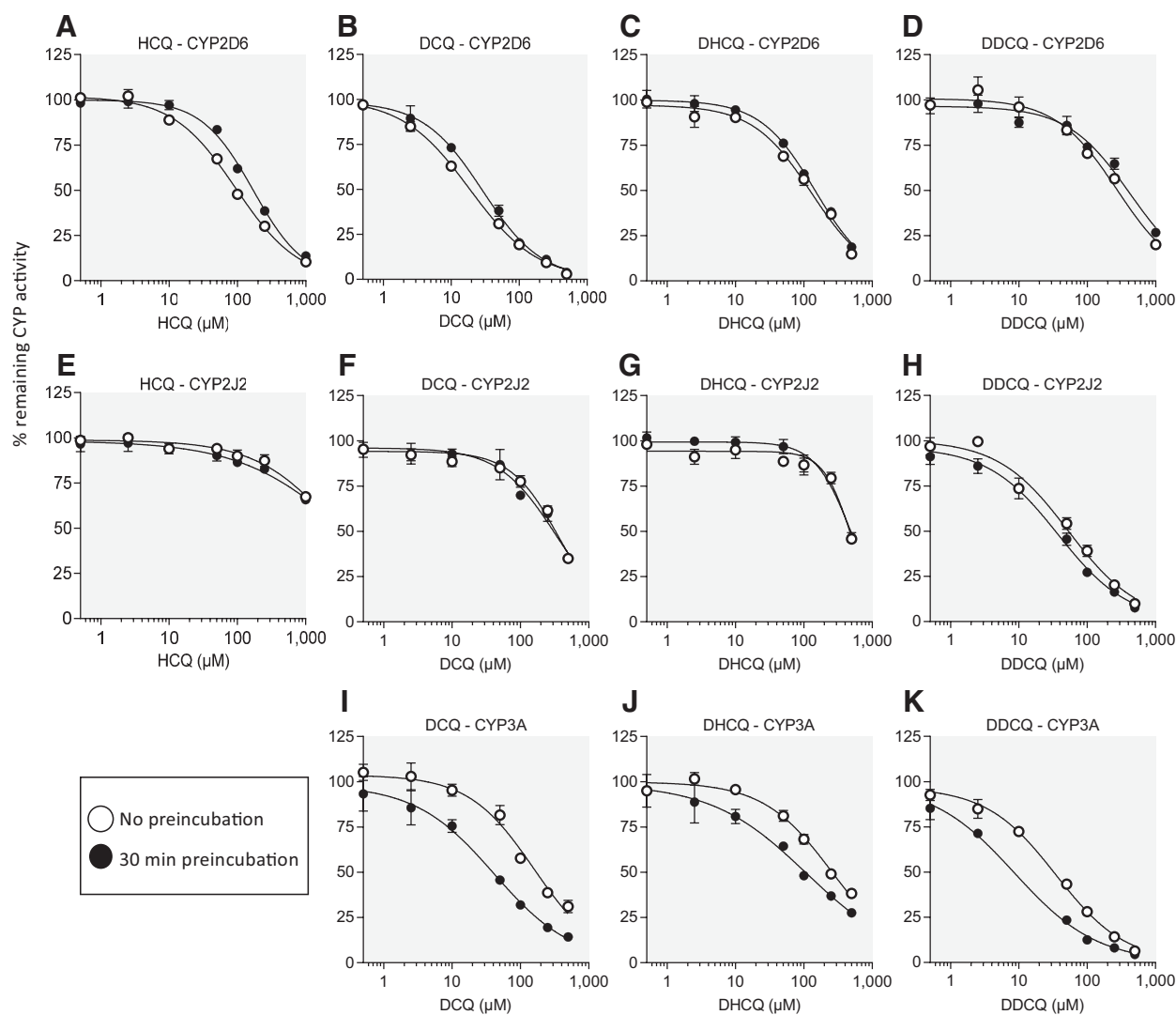
scaling method used (ISEF or CLISEF), different hepatic clearance values were obtained for CYP2D6 and CYP3A4. Of these, the CLISEF-based hepatic clearance values for CYP2D6 and CYP3A4 (1.6 and

TABLE 2

Inhibitory effects of HCQ, DCQ, DHCQ, and DDCQ on CYP activities in HLM incubations.  $IC_{50}$  values were determined following no preincubation (direct inhibition) or after a 30-min preincubation of inhibitor in the presence of NADPH (time-dependent inhibition), as described in Materials and Methods. A full table of the obtained results of the  $IC_{50}$  experiments (also showing lack of inhibition and the effects of BSA exclusion in cocktail 2) can be found in the supplement (Supplemental Table 5).  $IC_{50}$  values are reported as means of three determinations with their 95% confidence intervals.

Inhibitor	Enzyme	$IC_{50}$ ( $\mu$ M)		$IC_{50}$ shift
		Direct inhibition	Time-dependent inhibition	
HCQ	CYP2D6	91.2 (86.1–106)	170 (157–185)	<1.5
	CYP2J2	> 1,000	> 1,000	—
DCQ	CYP2D6	18.4 (17.5–20.2)	30.3 (24.7–33.1)	<1.5
	CYP2J2	374 (310–412)	341 (271–398)	<1.5
	CYP3A	149 (130–193)	45.8 (30.4–52.6)	3.2
DHCQ	CYP2D6	135 (109–149)	146 (134–158)	<1.5
	CYP2J2	504 (445–581)	491 (441–560)	<1.5
	CYP3A	260 (231–293)	117 (79.2–144)	2.2
DDCQ	CYP1A2	186 (139–203)	141 (60.7–168)	<1.5
	CYP2B6	182 (141–199)	199 (138–230)	<1.5
	CYP2C8	132 (115–143)	109 (62.1–122)	<1.5
	CYP2C9	107 (81.2–135)	87.7 (60.9–111)	<1.5
	CYP2C19	170 (93.2–206)	142 (30.5–202)	<1.5
	CYP2D6	54.7 (38.6–64.0)	90.9 (17.2–115)	<1.5
	CYP2J2	62.9 (41.9–70.8)	50.0 (9.3–64.2)	<1.5
	CYP3A	40.5 (25.7–45.0)	12.1 (5.0–14.2)	3.4

$IC_{50}$  shift,  $IC_{50}$  (direct inhibition)/ $IC_{50}$  (time-dependent inhibition) ratio.



**Fig. 5.** The inhibitory effects of HCQ, DCQ, DHCQ, and DDCQ on dextromethorphan *O*-demethylation (CYP2D6 probe reaction), astemizole *O*-demethylation (CYP2J2 probe reaction), and midazolam 1'-hydroxylation (CYP3A probe reaction) in HLM incubations.  $IC_{50}$  values were determined following no preincubation (direct inhibition) or after a 30-minute preincubation of inhibitor in the presence of NADPH (time-dependent inhibition), as described in Materials and Methods. The obtained  $IC_{50}$  values are given in Table 2. The data points show mean and standard deviations of measured CYP activity in inhibitor incubations as compared with that in solvent control incubations (triplicate incubations of one experiment). As the screening indicated no inhibition of CYP3A by HCQ, no CYP3A  $IC_{50}$  values were determined for HCQ.

1.5 l/h, respectively) were best in line with the microsomal-derived  $CL_H$  value (4.1 l/h). Unfortunately, we were unable to carry out CLISEF-based scaling of the CYP2C8  $CL_{int}$  value. Nevertheless, according to depletion and inhibition data, CYP2D6 and CYP3A4 seem to be equally important in the formation of DHCQ, whereas CYP3A4 plays a slightly larger role in DCQ formation. CYP2C8 seems to contribute slightly less, approximately 20–25% to both pathways.

There seems to be no published interaction studies investigating the effects of inhibitors of CYP2D6, CYP2C8, and CYP3A on the pharmacokinetics of HCQ. However, the DHCQ/HCQ ratio was associated with the CYP2D6 genotype in Korean lupus patients receiving HCQ (Lee et al., 2016). Another study did not find any significant association between CYP genotypes and HCQ response in British patients, although there was a trend for *CYP2C8\*3* and *CYP2C8\*4* to be associated with greater odds of response (Wahie et al., 2011).

Except for a study showing no reversible inhibition of CYP3A4 by HCQ (Li et al., 2020), little is known about the inhibitory effects

of HCQ on CYP enzymes *in vitro*. In our study, all three metabolites of HCQ inhibited CYP3A in a NADPH- and time-dependent fashion, as evidenced by  $IC_{50}$  shift values  $>1.5$  (Table 2). Their inactivation constants will be determined in a follow-up study, since time-dependent inhibition may cause a longer-lasting inhibitory effect, as compared with reversible inhibition. In addition, it may result in hapten formation and in some cases trigger an idiosyncratic adverse reaction (Kalgutkar et al., 2007). There seems to be little data on the effects of HCQ on CYP3A substrates *in vivo*, but HCQ has increased the plasma exposure of the CYP3A substrate MK-2206 by 16–92% in cancer patients (Mehnert et al., 2019).

In healthy subjects, HCQ has increased the plasma exposure of metoprolol by 65%, suggesting that it acts as an inhibitor of CYP2D6 (Somer et al., 2000). According to our data, HCQ and all of its three metabolites are reversible, competitive CYP2D6 inhibitors. DCQ was the most potent inhibitor with an  $IC_{50}$  value (18  $\mu$ M) more than 3-fold lower than those of the other compounds and a  $K_i$  value of 10.4  $\mu$ M



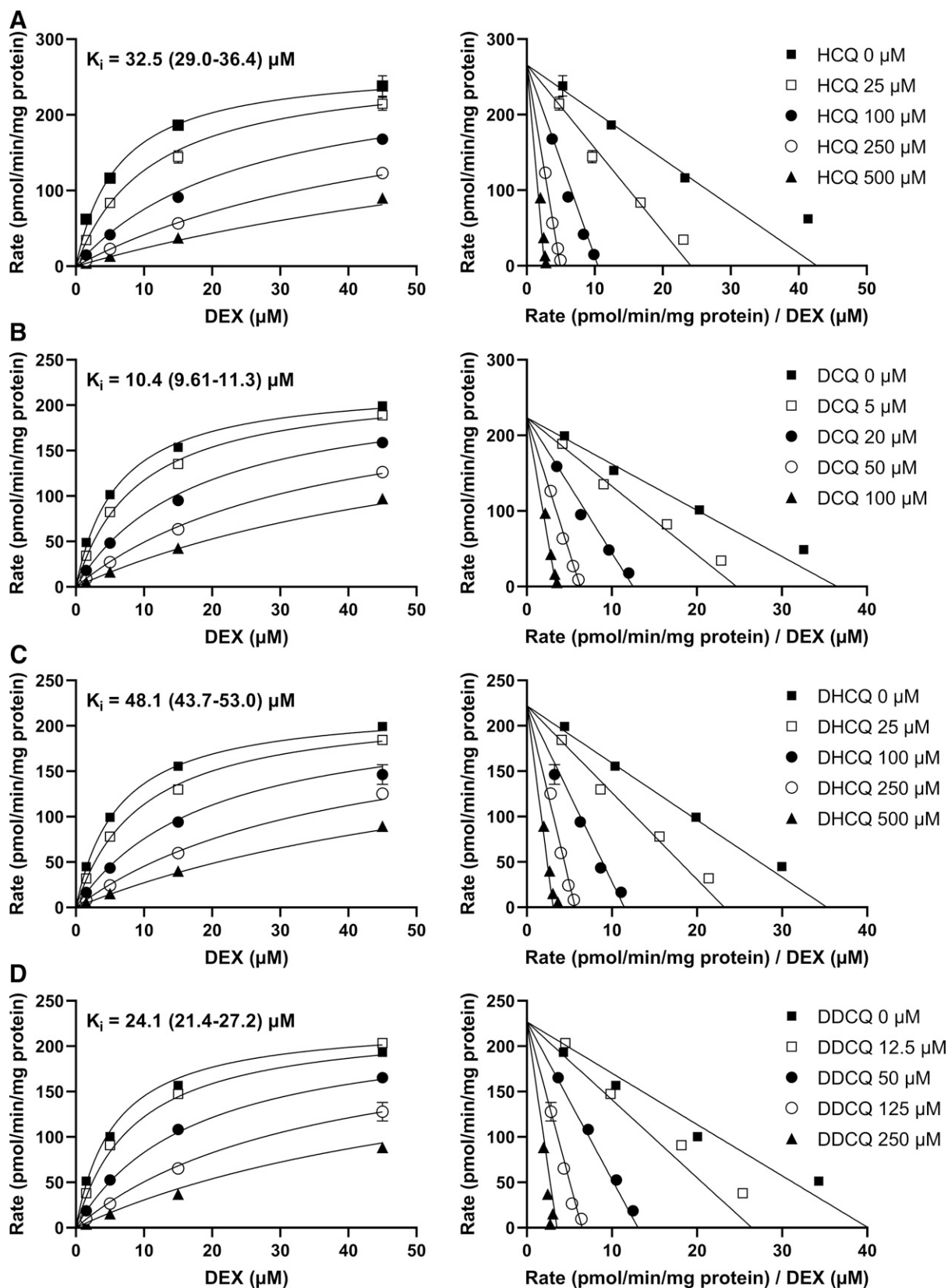


**Fig. 6.** Direct inhibition of dextromethorphan *O*-demethylation (CYP2D6 probe reaction) by HCQ, DCQ, DHCQ and DDCQ in HLM incubations. The rate of metabolite formation was assessed at four substrate concentrations over a range of inhibitor concentrations to determine  $K_i$  values as described in Materials and Methods. The data points show mean and standard deviations of measured rates of metabolite formation in inhibitor incubations as compared with that in solvent control incubations (triplicate incubations of one experiment). DEX, dextromethorphan.

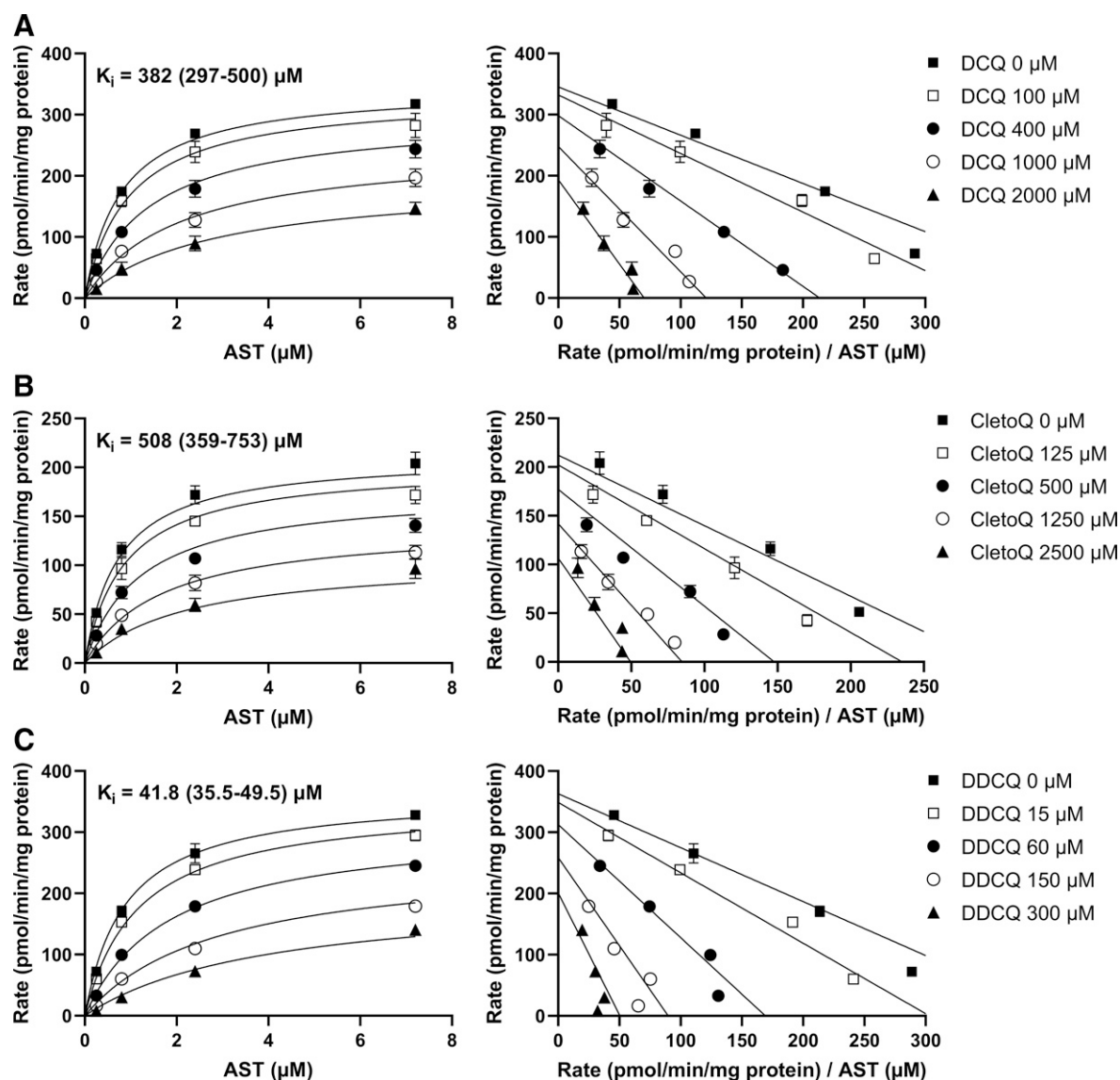


**Fig. 7.** Direct inhibition of astemizole *O*-demethylation (CYP2J2 probe reaction) by DCQ, DHCQ and DDCQ in HLM incubations. The rate of metabolite formation was assessed at four substrate concentrations over a range of inhibitor concentrations to determine  $K_i$  values as described in Materials and Methods. The data points show mean and standard deviations of measured rates of metabolite formation in inhibitor incubations as compared with that in solvent control incubations (triplicate incubations of one experiment). AST, astemizole.

(Fig. 6B). Static predictions based on the *in vitro* inhibitory data, however, suggested only a minimal (<1.1-fold) increase in metoprolol AUC when making the predictions using the total blood concentrations of HCQ measured at the end of the HCQ treatment in the clinical study (1.5–2.3  $\mu\text{M}$ ) or corresponding total plasma concentrations. However, HCQ and its metabolites accumulate extensively into tissues, indicating that their intracellular concentrations are higher than those in the blood stream. Accordingly, in predictions based on intracellular hepatocyte concentrations, estimated using mouse  $K_p$  or predicted human  $K_p$  values, we obtained much higher predicted AUC increases that were close to the observed interaction with metoprolol. Hence, our predictions suggest that the extensive accumulation of HCQ and its metabolites into tissues must be taken into account when predicting CYP-mediated interactions with HCQ as the perpetrator drug. Of note, the contribution of the metabolites to the total inhibitory effect was significant in all predictions. Nevertheless, the inhibitory effect of HCQ and its metabolites on CYP2D6 is of particular concern when used concomitantly with

CYP2D6 substrates that, similarly to HCQ, prolong QT interval, such as ondansetron and haloperidol. Moreover, autoinhibition of CYP2D6 may reduce its contribution to the overall metabolism of HCQ, thereby also increasing the relative importance of CYP2C8 and CYP3A4. To the best of our knowledge, there are no clinical reports to date suggesting time-dependent nonlinear pharmacokinetics for HCQ.

HCQ and its metabolites have very complex and unusual pharmacokinetic profiles. In addition to their extensive accumulation in blood and tissues, as a complicating factor, they display stereoselective pharmacokinetics and pharmacodynamics, as well as toxic properties (McChesney, 1983; McLachlan et al., 1993; Brocks et al., 1994; Ducharme et al., 1995; Lim et al., 2009). Unfortunately, the individual HCQ and metabolite enantiomers were not commercially available at the time of our study. Hence, the present *in vitro*  $CL_{int}$  and scaled hepatic clearance values reflect those of the racemic compounds. The present hepatic clearance (4.1 l/h) calculated based on the depletion of HCQ in HLMs approximates to 71% of the measured total intravenous

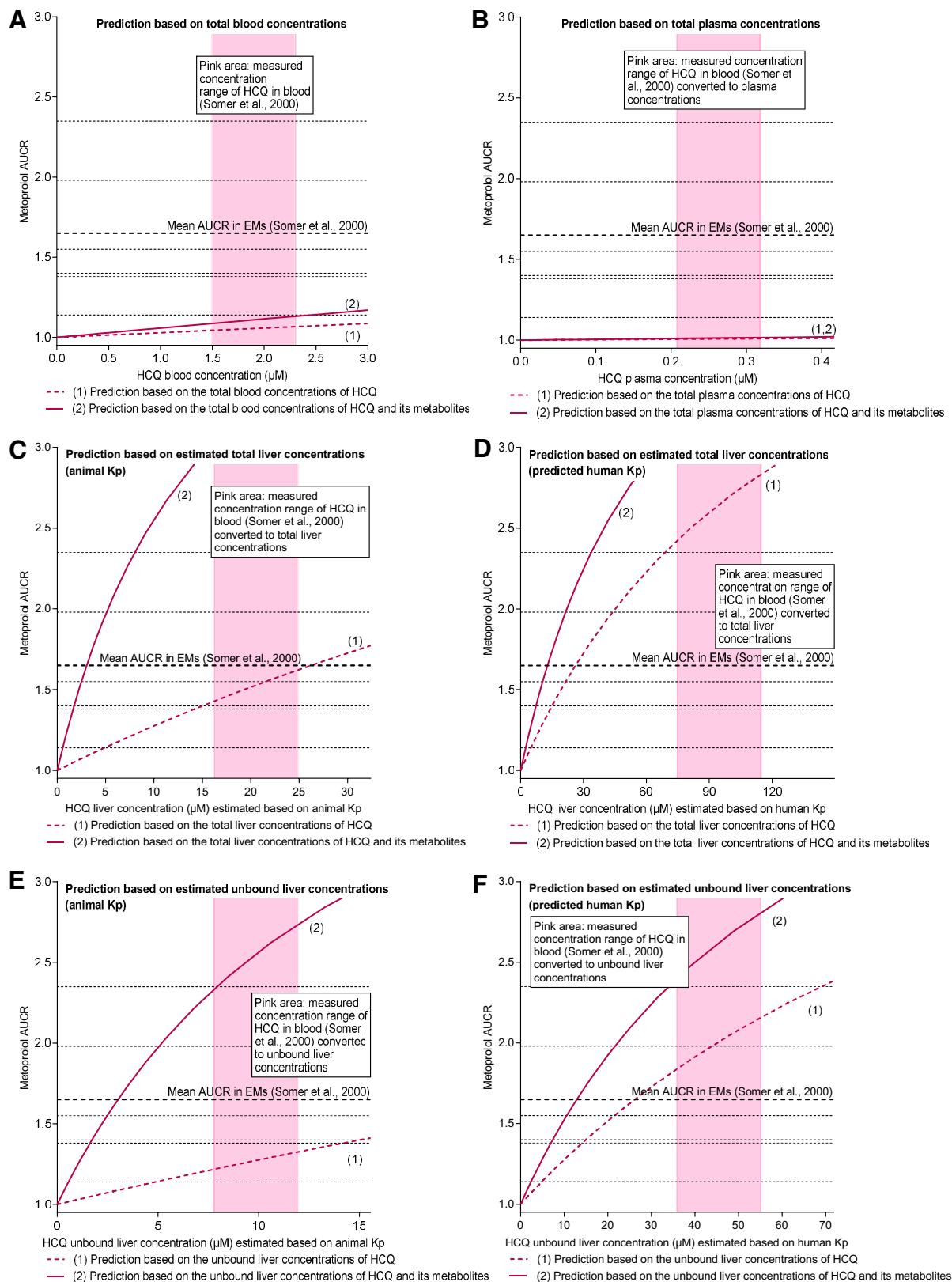


**Fig. 8.** Prediction of the total inhibitory effect of HCQ and its metabolites on the pharmacokinetics of the CYP2D6 substrate metoprolol in vivo. In a clinical interaction study between HCQ and metoprolol in six healthy volunteers, an eight-day treatment with HCQ increased the area under the plasma concentration-time curve (AUC) of a single dose of metoprolol (on day 9) by 1.65-fold (average fold increase indicated by the bold dashed line, with individual values ranging from 1.1 to 2.4 indicated by the dashed lines) (Somer et al., 2000). In the clinical study, HCQ blood concentrations were 1.5–2.3  $\mu\text{M}$  at single time points on days 8 and 9 (pink area). In predictions based on the present CYP2D6 direct  $K_i$  values and total blood (A) or plasma (B) concentrations of HCQ and its metabolites, HCQ concentrations of the measured magnitude did not explain the observed interaction (AUCR <1.1). When the predictions were based on estimated total liver concentrations (C–D), AUCR values of >2.9-fold were obtained. However, predictions based on unbound liver concentrations (E–F; assuming an unbound fraction in the hepatocytes that equals that observed in plasma for each compound), AUCR values of the clinically observed magnitude were obtained. A fraction metabolized by CYP2D6 ( $f_{m,CYP2D6}$ ) of 0.8 for metoprolol was used in the predictions, and several assumptions were made (Materials and Methods). Metoprolol AUCR, metoprolol AUC<sub>with HCQ</sub>/metoprolol AUC<sub>without HCQ</sub> ratio; EMs, extensive CYP2D6 metabolizers.

clearance (5.8 l/h). Our finding is in good agreement with clinical data showing that renal clearance accounts for approximately one third of the total plasma clearance of HCQ, whereas metabolism and biliary excretion is the predominant route of elimination (Tett et al., 1988; Tett et al., 1989).

Because of the complex pharmacokinetics of HCQ and the wide variability in its concentration profile, it has been difficult to relate measured HCQ concentrations to its therapeutic and adverse effects (Rainsford et al., 2015). Nevertheless, several pharmacokinetic and physiologically-based pharmacokinetic models have been developed for HCQ, in particular after the outbreak of COVID-19 (Collins et al., 2018; Themans et al., 2020; Idkaidek et al., 2021). Our data can be used to update these models, and to simulate the effects of CYP-mediated drug-drug interactions and variants in CYP genes. In addition to CYPs, HCQ interacts with drug transporters. HCQ is a substrate of P-glycoprotein in vitro (Weiss et al., 2020). There seem to be no studies investigating HCQ and transporter pharmacogenetics, but ATP-binding cassette transporter A4, organic anion transporting polypeptide (OATP) 1A2, and OATP1B1 have been associated with chloroquine pharmacokinetics and response (Grassmann et al., 2015; Sortica et al., 2017). With respect to transporter inhibition, HCQ does not affect the activities of breast cancer resistance protein, multidrug resistance-associated protein 1, organic anion transporter (OAT) 1, OAT3, OATP1B1, or OATP1B3 in vitro (Weiss et al., 2020; Telbisz et al., 2021; Yee et al., 2021). However, it is a potent inhibitor of multidrug and toxin extrusion proteins 1 and 2 (IC<sub>50</sub> 2–4 and 1–7 μM, respectively), and a moderate or weak inhibitor of P-glycoprotein (IC<sub>50</sub> 52 μM), organic cation transporter (OCT) 1 (IC<sub>50</sub> 20–47 μM), OCT2 (IC<sub>50</sub> ≥ 5 μM), OATP1A2 (IC<sub>50</sub> 9–19 μM), and OATP2B1 (IC<sub>50</sub> ≥ 84 μM) (Xu et al., 2016; Weiss et al., 2020; Martinez-Guerrero et al., 2021; Telbisz et al., 2021; Yee et al., 2021). Inhibition of OATP1A2 by HCQ in the retinal pigment epithelium has been suggested to contribute to the retinal degradation observed in patients using HCQ (Xu et al., 2016). Together, these novel transport data and our metabolism data can be combined in physiologically-based pharmacokinetic models to simulate the role of enzyme-transport interplay in HCQ pharmacokinetics.

In conclusion, the present study shows for the first time that CYP2D6, CYP3A4, and CYP2C8 are responsible for the in vitro metabolism of HCQ. Furthermore, our data indicate that HCQ and its metabolites are reversible, competitive inhibitors of CYP2D6, and that HCQ metabolites are mixed-type inhibitors of CYP2J2 and time-dependent inhibitors of CYP3A. The current data can thus be applied to improve physiologically-based pharmacokinetic models and update drug–drug interaction risk estimations for HCQ. Collectively, our findings contribute to an improved understanding of the clinical pharmacology of HCQ.

#### Acknowledgments

The authors thank Orion Corporation (Espoo, Finland) for providing hydroxychloroquine sulfate for *in vitro* experiments.

#### Authorship Contributions

*Participated in research design:* Backman, Filppula, Kahma, Kurkela, Niemi, Paludetto.

*Conducted experiments or drug concentration analysis:* Filppula, Kurkela, Paludetto.

*Performed data analysis:* Filppula, Kurkela, Paludetto.

*Wrote or contributed to the writing of the manuscript:* Backman, Filppula, Kahma, Kurkela, Niemi, Paludetto.

#### References

Brocks DR, Skeith KJ, Johnston C, Emamibafraji J, Davis P, Russell AS, and Jamali F (1994) Hematologic disposition of hydroxychloroquine enantiomers. *J Clin Pharmacol* **34**:1088–1097.

Charlier B, Pigeon M, Dal Piaz F, Conti V, Valentini G, Filippelli A, and Izzo V (2018) Development of a novel ion-pairing HPLC-FL method for the separation and quantification of hydroxychloroquine and its metabolites in whole blood. *Biomed Chromatogr* **32**:e4258.

Chhonker YS, Sleightholm RL, Li J, Oupický D, and Murry DJ (2018) Simultaneous quantitation of hydroxychloroquine and its metabolites in mouse blood and tissues using LC-ESI-MS/MS: An application for pharmacokinetic studies. *J Chromatogr B Analyt Technol Biomed Life Sci* **1072**:320–327.

Collins KP, Jackson KM, and Gustafson DL (2018) Hydroxychloroquine: A Physiologically-Based Pharmacokinetic Model in the Context of Cancer-Related Autophagy Modulation. *J Pharmacol Exp Ther* **365**:447–459.

Copeland R (2000) Modes of Reversible Inhibition, in *Enzymes: A Practical Introduction to Structure, Mechanism, and Data Analysis*, pp 270–282, Wiley-VCH, New York.

Ducharme J, Fieger H, Ducharme MP, Khalil SK, and Wainer IW (1995) Enantioselective disposition of hydroxychloroquine after a single oral dose of the racemate to healthy subjects. *Br J Clin Pharmacol* **40**:127–133.

FDA (2020) Coronavirus (COVID-19) Update: FDA Revokes Emergency Use Authorization for Chloroquine and Hydroxychloroquine. <https://www.fda.gov/news-events/press-announcements/coronavirus-covid-19-update-fda-revokes-emergency-use-authorization-chloroquine-and> (Last accessed Oct 26, 2022).

Grassmann F, Bergholz R, Mändl J, Jäggle H, Ruether K, and Weber BH (2015) Common synonymous variants in ABCA4 are protective for chloroquine induced maculopathy (toxic maculopathy). *BMC Ophthalmol* **15**:18.

Horby P, Mafham M, Linsell L, Bell JL, Staplin N, Emberson JR, Wiselka M, Ustianowski A, Elmahi E, Prudon B et al.; RECOVERY Collaborative Group (2020) Effect of Hydroxychloroquine in Hospitalized Patients with Covid-19. *N Engl J Med* **383**:2030–2040.

Idkaidek N, Hawari F, Dodin Y, and Obeidat N (2021) Development of a Physiologically-Based Pharmacokinetic (PBPK) Model of Nebulized Hydroxychloroquine for Pulmonary Delivery to COVID-19 Patients. *Drug Res (Stuttg)* **71**:250–256.

Kahma H, Aurinsalo L, Neuvonen M, Katajämäki J, Paludetto MN, Viinämäki J, Launiainen T, Filppula AM, Tornio A, Niemi M et al. (2021) An automated cocktail method for in vitro assessment of direct and time-dependent inhibition of nine major cytochrome P450 enzymes – application to establishing CYP2C8 inhibitor selectivity. *Eur J Pharm Sci* **162**:105810.

Kalgutkar AS, Obach RS, and Maurer TS (2007) Mechanism-based inactivation of cytochrome P450 enzymes: chemical mechanisms, structure-activity relationships and relationship to clinical drug-drug interactions and idiosyncratic adverse drug reactions. *Curr Drug Metab* **8**:407–447.

Kim KA, Park JY, Lee JS, and Lim S (2003) Cytochrome P450 2C8 and CYP3A4/5 are involved in chloroquine metabolism in human liver microsomes. *Arch Pharm Res* **26**:631–637.

Lee JY, Vinayagamorthy N, Han K, Kwok SK, Ju JH, Park KS, Jung SH, Park SW, Chung YJ, and Park SH (2016) Association of Polymorphisms of Cytochrome P450 2D6 With Blood Hydroxychloroquine Levels in Patients With Systemic Lupus Erythematosus. *Arthritis Rheumatol* **68**:184–190.

Li X, Höhl R, Sörgel F, and Fuhr U (2020) The parent drugs chloroquine and hydroxychloroquine do not inhibit human CYP3A activity in vitro. *Eur J Clin Pharmacol* **76**:1481–1482.

Lim HS, Im JS, Cho JY, Bae KS, Klein TA, Yeom JS, Kim TS, Choi JS, Jang JJ, and Park JW (2009) Pharmacokinetics of hydroxychloroquine and its clinical implications in chemoprophylaxis against malaria caused by Plasmodium vivax. *Antimicrob Agents Chemother* **53**:1468–1475.

Martinez-Guerrero L, Zhang X, Zorn KM, Ekins S, and Wright SH (2021) Cationic Compounds with SARS-CoV-2 Antiviral Activity and Their Interaction with Organic Cation Transporter/Multidrug and Toxin Extruder Secretory Transporters. *J Pharmacol Exp Ther* **379**:96–107.

McChesney EW (1983) Animal toxicity and pharmacokinetics of hydroxychloroquine sulfate. *Am J Med* **75** (1A):11–18.

McLachlan AJ, Cutler DJ, and Tett SE (1993) Plasma protein binding of the enantiomers of hydroxychloroquine and metabolites. *Eur J Clin Pharmacol* **44**:481–484.

Mehner JM, Kaveney AD, Malhotra J, Spencer K, Portal D, Goodin S, Tan AR, Aisner J, Moss RA, Lin H et al. (2019) A phase I trial of MK-2206 and hydroxychloroquine in patients with advanced solid tumors. *Cancer Chemother Pharmacol* **84**:899–907.

Munster T, Gibbs JP, Shen D, Baethge BA, Botstein GR, Caldwell J, Dietz F, Ettliger R, Golden HE, Lindsley H et al. (2002) Hydroxychloroquine concentration-response relationships in patients with rheumatoid arthritis. *Arthritis Rheum* **46**:1460–1469.

Pan H, Peto R, Henaio-Restrepo AM, Preziosi MP, Sathiyamoorthy V, Abdool Karim Q, Alejandria MM, Hernández García C, Kiény MP, Malekzadeh R et al.; WHO Solidarity Trial Consortium (2021) Repurposed Antiviral Drugs for Covid-19—Interim WHO Solidarity Trial Results. *N Engl J Med* **384**:497–511.

Pelkonen O and Turpeinen M (2007) In vitro–in vivo extrapolation of hepatic clearance: biological tools, scaling factors, model assumptions and correct concentrations. *Xenobiotica* **37**:1066–1089.

Plantone D and Koudriavtseva T (2018) Current and Future Use of Chloroquine and Hydroxychloroquine in Infectious, Immune, Neoplastic, and Neurological Diseases: A Mini-Review. *Clin Drug Investig* **38**:653–671.

Proctor NJ, Tucker GT, and Rostami-Hodjegan A (2004) Predicting drug clearance from recombinantly expressed CYPs: intersystem extrapolation factors. *Xenobiotica* **34**:151–178.

Projean D, Baune B, Farinotti R, Flinois JP, Beaune P, Taburet AM, and Ducharme J (2003) In vitro metabolism of chloroquine: identification of CYP2C8, CYP3A4, and CYP2D6 as the main isoforms catalyzing N-desethylchloroquine formation. *Drug Metab Dispos* **31**:748–754.

Rainsford KD, Parke AL, Clifford-Rashotte M, and Kean WF (2015) Therapy and pharmacological properties of hydroxychloroquine and chloroquine in treatment of systemic lupus erythematosus, rheumatoid arthritis and related diseases. *Inflammopharmacology* **23**:231–269.

Schrezenmeier E and Dörner T (2020) Mechanisms of action of hydroxychloroquine and chloroquine: implications for rheumatology. *Nat Rev Rheumatol* **16**:155–166.

Shimizu M, Furudate S, Nagai Y, Shimada K, Ohshima M, Setoguchi K, Hashiguchi M, and Yokogawa N (2022) Pharmacokinetics of hydroxychloroquine in Japanese systemic lupus erythematosus patients with renal impairment. *Mod Rheumatol* roac113 10.1093/mr/roac113.

Skipper CP, Pastick KA, Engen NW, Bangdiwala AS, Abbasi M, Lofgren SM, Williams DA, Okafor EC, Pullen MF, Nicol MR et al. (2020) Hydroxychloroquine in Nonhospitalized Adults With Early COVID-19: A Randomized Trial. *Ann Intern Med* **173**:623–631.

Somer M, Kallio J, Pesonen U, Pyykkö K, Huupponen R, and Scheinin M (2000) Influence of hydroxychloroquine on the bioavailability of oral metoprolol. *Br J Clin Pharmacol* **49**:549–554.

Sortica VA, Lindenau JD, Cunha MG, O Ohnishi MD, R Ventura AM, Ribeiro-Dos-Santos ÂK, Santos SE, Guimarães LS, and Hutz MH (2017) SLCO1A2, SLCO1B1 and SLCO2B1

- polymorphisms influences chloroquine and primaquine treatment in *Plasmodium vivax* malaria. *Pharmacogenomics* **18**:1393–1400.
- Telbisz Á, Ambrus C, Móznér O, Szabó E, Várady G, Bakos É, Sarkadi B, and Özvegy-Laczka C (2021) Interactions of Potential Anti-COVID-19 Compounds with Multispecific ABC and OATP Drug Transporters. *Pharmaceutics* **13**:81.
- Templeton IE, Chen Y, Mao J, Lin J, Yu H, Peters S, Shebley M, and Varma MV (2016) Quantitative Prediction of Drug-Drug Interactions Involving Inhibitory Metabolites in Drug Development: How Can Physiologically Based Pharmacokinetic Modeling Help? *CPT Pharmacometrics Syst Pharmacol* **5**:505–515.
- Tett S, McLachlan A, Day R, and Cutler D (1993) Insights from pharmacokinetic and pharmacodynamic studies of hydroxychloroquine. *Agents Actions Suppl* **44**:145–190.
- Tett SE, Cutler DJ, and Brown KF (1985) High-performance liquid chromatographic assay for hydroxychloroquine and metabolites in blood and plasma, using a stationary phase of poly(styrene divinylbenzene) and a mobile phase at pH 11, with fluorimetric detection. *J Chromatogr A* **344**:241–248.
- Tett SE, Cutler DJ, Day RO, and Brown KF (1988) A dose-ranging study of the pharmacokinetics of hydroxy-chloroquine following intravenous administration to healthy volunteers. *Br J Clin Pharmacol* **26**:303–313.
- Tett SE, Cutler DJ, Day RO, and Brown KF (1989) Bioavailability of hydroxychloroquine tablets in healthy volunteers. *Br J Clin Pharmacol* **27**:771–779.
- Thémans P, Belkhir L, Dauby N, Yombi JC, De Greef J, Delongie KA, Vandeputte M, Nasreddine R, Wittebole X, Guillaume F et al. (2020) Population Pharmacokinetics of Hydroxychloroquine in COVID-19 Patients: Implications for Dose Optimization. *Eur J Drug Metab Pharmacokinet* **45**:703–713.
- Ulander L, Tolppanen H, Hartman O, Rissanen TT, Paakkanen R, Kuusisto J, Anttonen O, Nieminen T, Yrjölä J, Ryssy R et al. (2021) Hydroxychloroquine reduces interleukin-6 levels after myocardial infarction: The randomized, double-blind, placebo-controlled OXI pilot trial. *Int J Cardiol* **337**:21–27.
- Wahie S, Daly AK, Cordell HJ, Goodfield MJ, Jones SK, Lovell CR, Carmichael AJ, Carr MM, Drummond A, Natarajan S et al. (2011) Clinical and pharmacogenetic influences on response to hydroxychloroquine in discoid lupus erythematosus: a retrospective cohort study. *J Invest Dermatol* **131**:1981–1986.
- Weiss J, Bajraktari-Sylejmani G, and Haefeli WE (2020) Interaction of Hydroxychloroquine with Pharmacokinetically Important Drug Transporters. *Pharmaceutics* **12**:919.
- White NJ, Watson JA, Hoglund RM, Chan XHS, Cheah PY, and Tarning J (2020) COVID-19 prevention and treatment: A critical analysis of chloroquine and hydroxychloroquine clinical pharmacology. *PLoS Med* **17**:e1003252.
- Xu C, Zhu L, Chan T, Lu X, Shen W, Madigan MC, Gillies MC, and Zhou F (2016) Chloroquine and Hydroxychloroquine Are Novel Inhibitors of Human Organic Anion Transporting Polypeptide 1A2. *J Pharm Sci* **105**:884–890.
- Yang J, Jamei M, Yeo KR, Rostami-Hodjegan A, and Tucker GT (2007) Misuse of the well-stirred model of hepatic drug clearance. *Drug Metab Dispos* **35**:501–502.
- Yee SW, Vora B, Oskotsky T, Zou L, Jakobsen S, Enogieru OJ, Koleske ML, Kosti I, Rödin M, Sirota M et al. (2021) Drugs in COVID-19 Clinical Trials: Predicting Transporter-Mediated Drug-Drug Interactions Using In Vitro Assays and Real-World Data. *Clin Pharmacol Ther* **110**:108–122.

---

**Address correspondence to:** Anne M. Filppula, Department of Clinical Pharmacology, PO Box 20 (Tukholmankatu 8 C), 00014 University of Helsinki, Finland. E-mail: [anne.filppula@abo.fi](mailto:anne.filppula@abo.fi)

---